The Critical Heat Flux Condition With Water in a Uniformly Heated Microtube

A. P. Roday

T. Borca-Tasçiuc

M. K. Jensen[1]
e-mail: JenseM@rpi.edu

Department of Mechanical, Aerospace and Nuclear Engineering,
Rensselaer Polytechnic Institute,
Troy, NY 12180-3590

The critical heat flux (CHF) condition needs to be well understood for designing miniature devices involving two-phase flow. Experiments were performed to determine the CHF condition for a single stainless steel tube having an inside diameter of 0.427 mm *subjected to uniform heat flux boundary conditions. The effects of mass flux, pressure, and exit quality on the CHF were investigated. The experimental results show that the CHF increases with an increase in mass flux and exit pressure. For all exit pressures, the CHF decreased with an increase in quality in the subcooled region, but with a further increase in quality (near zero quality and above), the CHF was found to have an increasing trend with quality (up to about 25% quality). CHF values in this region were much higher than those in the subcooled region. This suggests that even at very low qualities, the void fraction becomes appreciable, which results in an increase in the average velocity, thereby increasing the CHF limit.* [DOI: 10.1115/1.2780181]

Keywords: CHF, boiling, exit quality, subcooled, saturated, microtube

1 Introduction

For more than a decade, one of the important applications of heat transfer engineering has been thermal management of electronic devices, and this is a result of the continuous and rapid development of integrated circuit technology. Moore's law [1] states that the number of transistors in an integrated circuit (IC) doubles every 18 months. Due to the increased packaging density and performance of microelectronic devices, IC chip power has significantly risen in the last two decades. The heat fluxes in these devices are high, from about 50 W/cm^2 in the current electronic chips to about 2000 W/cm^2 [2] in semiconductor lasers.

The challenge in cooling such devices is that the chip temperature has to be maintained below 85 °C despite the high local heat flux. Such a high heat flux imposes a practical limit on traditional cooling approaches such as natural and forced convection using air. Adoption of liquid cooling in packaging of electronic devices seems to be a viable option as it offers the capability of heat removal rates much higher (more than four times) than that of air cooling. Also, the cooling could be accomplished with or without phase change of the liquid (coolant). The use of two-phase cooling has many attractive features from a thermal perspective, such as reduced flow rate requirements while removing large amounts of heat and operating with lower temperature differences. Hence, two-phase cooling approaches at the small scale have become important; with the current trends in the advancement of microelectromechanical system (MEMS) technology, the fabrication of components for liquid cooling could become more cost effective.

With the development of nanotechnology and fuel-cell technology, more compact and enhanced heat exchangers are being designed with surface area densities as high as 10,000 m^2/m^3 [3]. Such devices could be useful as fuel reformers in automotive fuel cells, in air separation and cryogenic industries, and in the aerospace industry to reduce weight. The high surface densities associated with these heat exchangers can be achieved by construction techniques that result in a large number of small channels in the 100–1000 μm range [4]. Therefore, mini- and microscale heat transfer is becoming important in such industrial heat exchangers as well. Thus, we see that two-phase heat transfer in such small channels is a potential solution to thermal control (cooling) and thermal processing applications (compact heat exchangers).

Flow boiling in tubes and channels is a complex convective phase change process. In cases where the system is heat flux controlled (electrical heating or nuclear heating), an increase in heat flux ultimately leads to deterioration in heat transfer, often indicated by a sudden sharp rise in the wall temperature or the physical burnout of the wall. This upper limit on the heat flux is defined as the critical heat flux (CHF) condition, and engineers must take this into consideration when designing heat transfer equipment for safe operation. There has been a growing interest to understand the CHF behavior in small micron-sized passages and also to determine if this CHF behavior is similar to that observed in large-sized tubes and channels. Unfortunately, the literature so far has been inconclusive in understanding the parametric effects on the CHF condition. This is partly due to the difficulty in carrying out experiments at the small scale. Some of the existing literature on CHF in mini- and microchannels is reviewed here.

2 Critical Heat Flux Studies in Mini/Microchannels

There are very few investigations of CHF studies in small circular tubes. There have been some studies in tubes with small dimensions (down to about 0.3 mm) involving very high mass velocities intended for extremely high heat flux removal as in fusion reactors [5,6], but studies at lower mass fluxes are very limited. Celata et al. [7] have conducted subcooled CHF studies in tube diameters as small as 0.25 mm, but these were, again, for very high heat fluxes (up to 70 MW/m^2) and high mass fluxes (greater than 5000 kg/m^2 s) in the fusion technology application.

Nariai et al. [8] reported CHF studies with water at ambient exit pressure in stainless steel tubes with inside diameters of 1 mm, 2 mm, and 3 mm; tests were performed from the subcooled to the quality region (very close to zero quality) for mass fluxes ranging from 7000 to 11,000 kg/m^2 s. The inlet water temperature was between 17 °C and 80 °C. They indicated that the CHF decreased with an increase in exit quality in the subcooled region (i.e., negative quality indicated subcooled liquid). There was a minimum in the CHF versus quality curve very close to zero quality. As quality

[1]Corresponding author.

Contributed by the Heat Transfer Division of ASME for publication in the JOURNAL OF HEAT TRANSFER. Manuscript received January 4, 2007; final manuscript received May 11, 2007; published online January 28, 2008. Review conducted by Anthony M. Jacobi.

was further increased to a positive value, the CHF increased sharply. The maximum exit quality in their data was about 0.05.

A similar trend was observed by Bergles and Rohsenow [9] for CHF with de-ionized water in a stainless steel 2.38 mm tube with $L/D=15$, mass flux of 3000 kg/m^2 s, and an exit pressure of 207 kPa. At high subcooling, CHF decreased monotonically with increases in quality; the data then passed through a minimum and then increased in the bulk boiling region. It was argued that at low values of subcooling, the void fraction became appreciable, which caused an increase in average velocity with the result that the burnout limit was raised. They found a strong inverse dependence of CHF on diameter. They referred to earlier work by other researchers who believed that CHF decreased with decrease in diameter when the size was reduced below 2 mm and suggested that this could be due to flow oscillations.

Roach et al. [10] studied the CHF associated with flow boiling of subcooled water in circular tubes with diameters of 1.17 mm and 1.45 mm ($L/D=110$), mass velocities from 250 kg/m^2 s to 1000 kg/m^2 s, exit pressures from 345 kPa to 1035 kPa, and inlet temperatures from 49 °C to 72 °C. They observed the CHF condition at very high exit qualities (around 0.8) indicating dryout. CHF increased with increasing channel diameter, mass flux, and pressure. They found that in both the tube sizes for pressure around 690 kPa and mass flux about 800 kg/m^2 s, CHF did not occur at all, and a smooth transition from nucleate to film boiling took place. The deviation for the smaller tube from the Bowring correlation was about 35% for most heat flux values; it should be noted that the Bowring correlation was based on data with diameters from 2 mm to 45 mm.

Oh and Englert [11] conducted subatmospheric CHF experiments with water in a single rectangular aluminum channel heated on one side with electric strip heaters. Their channel cross-section dimensions were 1.98×50.8 mm^2 (hydraulic diameter of 3.8 mm) and heated length of 600 mm ($L/D=160$). The exit pressures ranged from 20 kPa to 85 kPa. The tests were performed with low mass fluxes from 30 kg/m^2 s to 80 kg/m^2 s. CHF was found to increase with mass flux, in almost a linear fashion. The relation between subcooling and CHF was also found to be linear although the effect was not significant. Between an inlet subcooling of 44–66 °C, CHF increase was just 15%. Experimental CHF data did not match well with the predicted CHF from existing low flow-rate correlations. The closest prediction of the CHF data was with the Lowdermilk correlation [12], which underpredicted the data by about 30%.

CHF experiments were performed by Lazarek and Black [13] with R-113 in a stainless steel tube of inside diameter 3.15 mm ($L/D=40$) in a vertical orientation. The pressure was varied from 124 kPa to 413 kPa. The mass velocities were in the range of 140–740 kg/m^2 s. Inlet subcooling varied between 3 °C and 73 °C. Following the power increase, the wall temperatures underwent progressively large oscillations due to intermittent rewetting of the passage wall. CHF occurred because of the dryout of the liquid and always at the exit of the heated test-section length. Axial conduction effects on CHF were not assessed in this study even though the test section had a thick wall (0.4 mm).

Bowers and Mudawar [14] conducted studies with R-113 in circular minichannel and microchannel heat sinks machined into large copper blocks. Three parallel channels 2.54 mm diameter each formed the minichannel heat sink. The microchannel heat sink had 510 μm diameter channels. They concluded that the CHF was not a function of inlet subcooling in either the mini- or microchannel heat sink.

Yu et al. [15] carried out CHF experiments with water in a stainless steel 2.98 mm inside diameter tube ($L_h/D=305$) and a pressure of about 207 kPa. The outside diameter of the test section was 4.76 mm. CHF was found to decrease with a decrease in mass flux (mass fluxes varied between 50 kg/m^2 s and 200 kg/m^2 s). CHF qualities were found to be relatively high, above 0.5. Kamidis and Ravigururajan [16] used R-113 to investigate the CHF condition in 1.59 mm, 2.78 mm, 3.97 mm, and 4.62 mm short tubes (L/D ranged from 11 to 24). CHF was found to increase with mass velocity.

Lezzi et al. [17] reported experimental results on CHF in forced convection boiling of water in a horizontal tube of diameter 1 mm and $L/D=250$, 500, and 1000. The tube wall thickness was 0.25 mm. The mass flux varied between 800 kg/m^2 s and 2700 kg/m^2 s. In all cases the quality at the outlet was high (greater than 0.6), and the CHF was reached through dryout. They concluded that for low mass fluxes and tube diameters down to 1 mm, the effect of the diameter on CHF did not differ from the characteristics of the large diameter tubes. They claimed that no oscillations affected the data, but data on pressure were not reported. Also, conduction along the thick tube wall could significantly affect the CHF. This effect was not assessed in this study.

Jiang et al. [18] conducted CHF studies with water with an array of V-grooved microchannels of either 35 or 58 channels each of 40 μm hydraulic diameter and either 10 or 34 channels of 80 μm hydraulic diameter. In all the devices tested, the wall temperature increased almost linearly with heat flux until the onset of the CHF condition. The quality at the exit was 1.0 at CHF, indicating a single-phase flow of the vapor. CHF was found to be a function of the flow rate, and CHF increased linearly with an increase in the rate of flow.

Recently, Wojtan et al. [19] investigated saturated CHF in a single uniformly heated microchannel of 0.5 mm and 0.8 mm internal diameters using R-134a and R-245fa. They did not find any influence of inlet subcooling on CHF; at the same mass flux, CHF increased with increasing diameter, which is the opposite effect found by Bergles and Rohsenow [9] whose study covered the subcooled to the saturated region (up to qualities of about 0.12). Wojtan et al. studied the effect of exit quality on CHF only for qualities above 40%. They presented a new correlation to predict CHF in circular uniformly heated microchannel.

Kuan and Kandlikar [20] studied the effect of flow boiling stability on CHF with R-123 in six parallel microchannels (cross-sectional area of each microchannel is 1054×157 μm^2) machined on a copper block of dimensions 88.9×29.6 mm^2. They developed a theoretical model to represent the CHF mechanism and correlated it with their experimental data.

Koşar et al. [21] obtained a few CHF data with de-ionized water flowing through five parallel microchannels (227 μm hydraulic diameter) micromachined on a silicon wafer. They concluded that the exit pressure did not have any effect on the dependence of CHF, but the CHF was found to increase with an increase in mass velocity. The CHF seemed to decrease with an increase in exit quality (for qualities above 0.5), although there was an upward jump at about $x=0.7$.

Zhang et al. [22] evaluated existing correlations for flow boiling of water with available databases from small diameter tubes and developed a new correlation based on the inlet conditions by doing parametric trend analyses of the collected database.

Thus, there is no general agreement on the mini/microchannel CHF studies conducted so far. For example, in minichannels, Roach et al. [10] found the CHF to increase with increasing channel diameter but Bergles and Rohsenow [9] found an inverse dependence of diameter on CHF. Oh and Englert [11] found a weak linear relationship between inlet subcooling and CHF, but Bowers and Mudawar [14] found that the CHF was not at all affected by the inlet subcooling during their studies in parallel microchannels. Wojtan et al. [19] found, in their studies with single tubes, that the CHF was not dependent on inlet subcooling. The data by Yu et al. [15] indicated that the CHF increased with an increase in exit quality, but the data by Wojtan et al. [19] depicted the opposite effect. The CHF studies by Roach et al. [10] show that the CHF increases with increasing pressure, but the data in some studies [19] do not show a strong dependence of pressure on CHF. Studies such as Refs. [8,9] show that the CHF increases from the

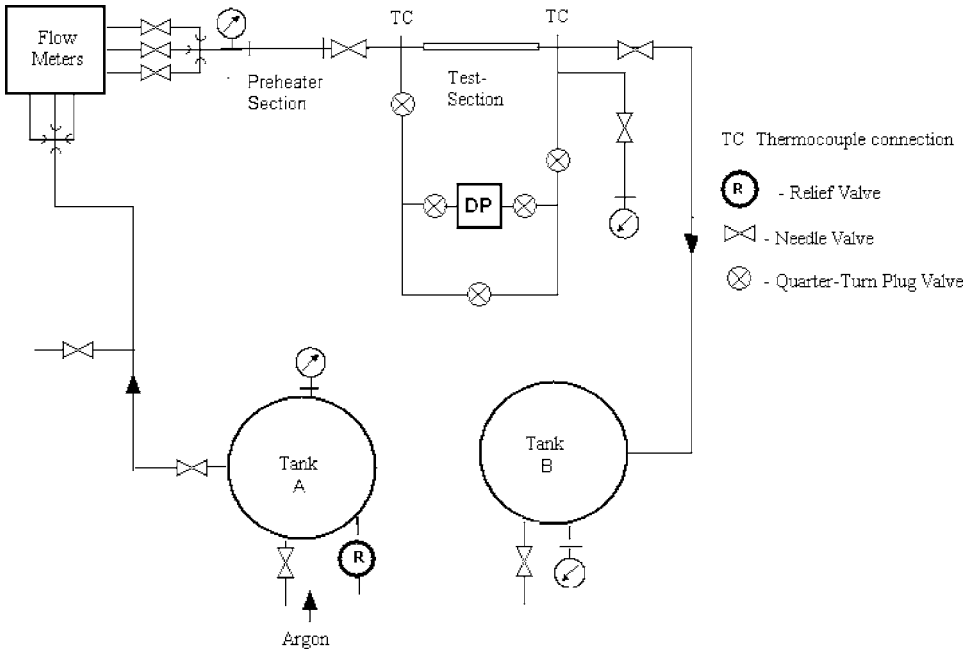

Fig. 1 Description of test facility

subcooled to the saturated region near zero qualities, but other studies have not reported this behavior. Many researchers have attempted to correlate their data with the existing correlations, but the different data vary in the degree of disagreement. Many different correlations have been developed, but they are mostly applicable to the limited data range over which the experiments were conducted.

Overall, there are very limited studies on CHF in the micron-sized dimensions. There are very few studies for CHF at subatmospheric pressures, close to ambient pressure with low mass fluxes, or with tube diameters below 1000 μm. Most of the studies in the microscale range use parallel rectangular microchannels. Such channels are subject to instabilities and conduction through the block on which the channels are machined, and these conditions affect the CHF condition. Hence, the objective of this paper is to experimentally investigate the effects of mass flux, inlet subcooling, exit quality, and pressure on the CHF condition for a single stainless steel microtube. The tube internal diameter used in this study is 0.427 mm with an outside diameter of 0.55 mm and a heated length of 59 mm. A range of mass fluxes (315–1570 kg/ms^2), inlet subcoolings (2–50°C), and exit pressures (25.3–179 kPa) was examined during this study.

3 Experimental Facility and Test Section

3.1 Experimental Facility. The experimental investigations were carried out using the test facility as shown in Fig. 1, which facilitated the flow of water between Tank A and Tank B. The major components of the loop are the two tanks, flowmeters, preheater, test-section assembly, and the pressure transducer arrangement. Water was stored in Tank A, which was equipped with a vacuuming, pressurizing, and a degassing arrangement. As a safety measure, a pressure relief valve was also provided on the tank. Water was circulated in the loop by imposing a pressure difference between the two tanks. Water passed through one of the three rotameters depending on the flow range, and the flow was set by an in-line needle valve. A pressure gauge measured the pressure at the inlet of the preheater section. The water was heated to a desired temperature by passing it through a 200 mm long preheater section. This preheater was constructed by coiling resistance wire around 6.4 mm stainless steel tube. Voltage was applied to the wire through a variable transformer. The preheated fluid was throttled before it entered the test section. The test section was mounted on an assembly, which facilitated quick replacement of the test section. Detailed discussion of the test section and its mounting is provided later. A differential pressure transducer measured the pressure drop across the test-section length. A Bourdon-type pressure gauge recorded the pressure at the exit of the test section. Following the test section, the fluid entered Tank B from where it was later pumped back to the main storage Tank A.

3.2 Test Section and Guard Heater. The test sections were individual hypodermic tubes made of 304 stainless steel cut from a longer piece of tubing. The test-section ends were sanded and polished on a sander using 400 and 600 grit sand paper, and the final polishing was carried out using a 1 μm diamond solution. Microscopic examination of the test section so prepared ensured that no burrs were present. The test section was heated by passing dc through it. For this purpose, 2×2 cm^2 brass strips were soldered at two different locations on the hypodermic tubing and are shown in Fig. 2; electric power wires were soldered on these strips. The voltage to the test section was provided through a dc power supply with variable output between 0 V and 10 V and a current rating of 0–100 A. The test section was held at its two ends using compression fittings. These fittings housed a Teflon bushing through which the test-section tubing was inserted. Once the test section was inserted, the fitting was tightened to create a leak-tight joint.

The test section was housed inside a guard heater to minimize heat losses during diabatic experiments. A 2.0 cm thick layer of insulation was wrapped around this test section. A 5 cm diameter copper tube, with resistance wire and a thermocouple bonded to it, was secured over this insulation. Then, another 3 cm layer of insulation was wrapped around the copper tube. The guard heater covered the area from compression fitting to compression fitting. The power to this guard heater was controlled through a variable transformer.

T-type thermocouples were mounted at six different locations on the test section for wall temperature measurements. Thermocouples nearer to the exit of the heated section were spaced 1.8 mm apart to better track the CHF condition. Also, one ther-

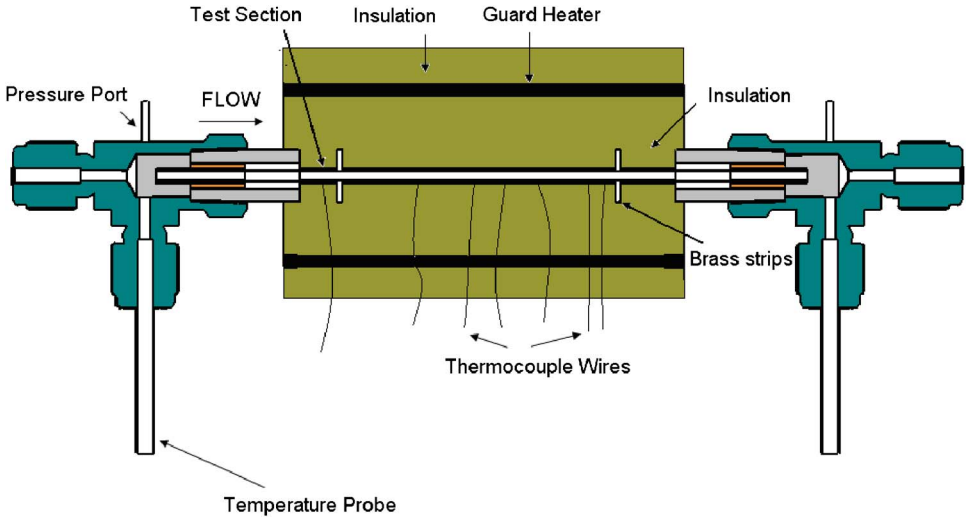

Fig. 2 Test Section Assembly

mocouple was mounted on the test section ahead of the heated length to check for any backflow of vapor and axial conduction away from the heated section. Pressure taps were provided at the two ends of the test section (about 35 mm away from the heated section). Temperature probes measured the temperature of water at the inlet and exit of the test section at the same location as the pressure taps. The inlet and exit portions of the test section were heavily insulated to avoid heat loss.

4 Instrumentation

Five types of measurements were made: temperature, flow rate, pressure, voltage, and geometry of test section (diameter and length).

Temperature measurements. Two different temperature measurements were needed, that of the test-section wall and the working fluid. The wall temperatures were measured using thermocouples made of fine wire (36 AWG, 0.127 mm wire diameter) with beads welded in an inert environment. The inlet and outlet fluid temperatures were measured using probes made from thermocouples to avoid heat conduction through the probe. The accuracy of the temperature measurement using these thermocouples was $\pm 0.3\,^{\circ}\mathrm{C}$.

Flow-rate measurement. The flow rate was measured using rotameters. The flowmeter was mounted between the tank and the preheater. To cover the entire range of flow rates needed for the experimentation, a bank of three flowmeters was used. This increased the accuracy of measurement. The accuracy of flow measurement was $\pm 2.0\%$ of the reading.

Pressure measurement. There are two different types of pressure measurements performed during the experiments: pressure level and pressure drop across the test-section length. The pressure level was measured with Bourdon-type pressure gauges at the outlet of the flowmeter and at the exit of the test section. As seen in Fig. 2, the pressure taps were provided outside the test section and were connected to the differential pressure transducer. This transducer measured the total pressure drop across the test-section overall length. The pressure taps were mounted very close to the test-section exit, about 5 mm from the test-section end (35 mm from the heated section). The differential pressure transducer had an accuracy of $\pm 0.25\%$ of full scale. The diaphragm used during these tests had a full scale pressure reading of 86 kPa.

Test-section geometry (diameter and length) measurements. The diameter of the test section used in the experiment was carefully measured using a Unitron optical microscope with a $40\times$ magnification and having a Mitutoyo measuring probe attachment. The length of the test section was measured using vernier calipers. The accuracy in measuring the diameter was ± 0.00254 mm and on the length was ± 0.03 mm.

Voltage measurement. Power supplied to the test section was measured by taking voltage measurements across the test section and a current shunt sized to ensure high accuracy depending on the current range. The accuracy of the shunts was $\pm 0.25\%$.

Data acquisition system. The outputs from all the instruments were recorded for every experimental run. Manual readings were taken from the flowmeters and the pressure gauges. All other data were directly read through a computerized data acquisition system using LABVIEW® software and National Instruments data acquisition and conditioning hardware. A solid-state relay was used to shut off the test-section power when the CHF condition was reached. Two thermocouples nearest to the outlet of the test section were monitored, and once the wall temperature reached a predetermined value, power was cut to the test section. This shutoff ensured that the test section was saved for further experiments. The data acquisition system had the capability of gathering data up to 1000 Hz. The accuracy of voltage measurement was $\pm 0.07\%$. Computer programs for data acquisition and reduction were developed to control the acquisition, reduction, and storage of data.

5 Experimental Procedures

Calibration of the flowmeters was done using the weigh tank technique of measuring the volume of fluid collected in a given amount of time. Calibration of the Bourdon-type pressure gauges was done using a deadweight tester. The differential pressure transducers were calibrated for each diaphragm using a water column over the full pressure range of the transducers.

Water was degassed before circulating in the loop. This was done by passing high pressure argon (an inert gas) through the water stored in Tank A. This gas stripped the dissolved oxygen from water. The process was carried out in vacuum so that the dissolved gases along with the inert gas are pulled out leaving the tank with degassed water. The measured oxygen content was 2.2 ppm.

For an experimental run, the flow was set to the desired value by adjusting the in-line valves. The exit pressure was set by controlling the pressure in Tank B. The preheater and guard heater were turned on and set to the desired values. A criterion of a maximum $\pm 0.5\,^{\circ}\mathrm{C}$ variation in wall temperatures in about 15 min was set to detect the quasisteady state as the wall temperatures remained fairly constant after about 15 min, indicating that a steady state was attained. It took up to about 2 h to reach the initial quasisteady state depending on the operating conditions and

about 30 min for each new setting of the flow rate. For every new setting of the inlet temperature, it took another 1 h for the flow to reach steady state. Once the steady state was reached, data were recorded for the set operating conditions.

A single-phase experiment was first performed and the heat loss was estimated by comparing the sensible heat gained by the water (inlet and outlet water temperatures were measured during the experiment) with the power input to the test section. This experiment was done by setting the power to the test section at a particular value and adjusting the guard heater power so that the guard heater temperature was only slightly above the wall temperature on the test section. This ensured minimum heat loss from the test-section wall. The measurements of flow, temperature, and voltages were then recorded.

Next, the guard heater temperature was set close to the saturation temperature (corresponding to the outlet pressure). The inlet fluid temperature was again set to the desired value, steady state was reached, and then the power to the test section was increased in progressively smaller increments until the CHF condition was reached. This condition was marked by a nearly instantaneous rise (the switching time of the relay is about 7 ms) in the wall temperature of about 80–100 °C over the saturation temperature.

6 Data Reduction

The measured quantities are the total pressure drop ($\Delta p_{t,\text{expt}}$) from the differential pressure transducer, the volumetric flow rate (Q) from the flowmeter, the test section inside diameter (D), the test-section length (L), the voltage across the shunt (V_{sh}), the voltage across the test section (V_{TS}), the heated length of the test section (L_h), the fluid inlet temperature ($T_{f,i}$), the fluid exit temperature ($T_{f,o}$), and the exit pressure (P_{exit}).

Power to the test section is calculated by the following equation:

$$\text{PW}_{\text{TS}} = V_{\text{TS}} I \tag{1}$$

where V_{TS} is the voltage across the test section and I is the current through the test section. The current to the test section was obtained from the current shunt voltage measurement.

Heat loss was estimated by comparing the sensible heat gained by the water in single-phase experiments, which is given by

$$H = \rho Q c_p (T_{f,o} - T_{f,i}) \tag{2}$$

with the electric power input over a wide range of flow rates (Re ranging from 250 to 1200). The guard heater ensured that the heat loss was within ±5%. During the two-phase experiments, the guard heater temperature was set slightly higher than the fluid saturation temperature, and it is assumed that the heat loss was similar to that observed during the single-phase tests.

The heat flux was obtained by

$$q'' = 1000 P W_{\text{TS}} / \pi D L_h \tag{3}$$

The wall superheat is obtained as

$$\Delta T_{\text{sat}} = T_{w,\text{in}} - T_{\text{sat}} \tag{4}$$

The fluid saturation temperature (T_{sat}) is that corresponding to the measured exit pressure. This was compared with the measured fluid temperature at the outlet of the test section and excellent agreement with the measured and calculated temperatures was obtained. The local inner wall temperature is obtained from the outer wall temperature using a 1D heat conduction model assuming steady-state radial conduction through the wall with uniform heat generation and no heat losses.

The mass flow rate is given by

$$\dot{m} = \rho Q \tag{5}$$

and the mass flux is defined as

$$G = 10^6 \dot{m} / (\pi D^2 / 4) \tag{6}$$

Table 1 Experimental conditions for the CHF study

Parameter	Range
Fluid	De-ionized, degassed water (~2.2 ppm O_2)
D/D_{out}	0.427 mm/0.550 mm
L_h (mm)	59
P_{exit} (kPa)	179, 102, 25.3
G (kg/m^2 s)	315, 560, 870, 1570
ΔT_{sub} (°C)	2–50

Exit quality was obtained from an energy balance between the heat supplied to the test section and the heat gained by the fluid. In the case of subcooled exit flow, enthalpy of the fluid [$h(T)$] is the liquid enthalpy corresponding to that temperature. Thus, the exit quality for a subcooled liquid is defined as

$$x = \frac{h(T) - h_f(P)}{h_{fg}(P)} \tag{7}$$

where h_{fg} is the enthalpy of vaporization corresponding to the exit pressure and h_f is the saturated liquid enthalpy corresponding to the exit pressure.

In the case of an exit flow in the saturation region, the quality is calculated by

$$x = \frac{1}{h_{fg}} \left[\frac{10004 L_h q''}{GD} - c_p (T_{\text{sat}} - T_{f,i}) \right] \tag{8}$$

7 Uncertainty Analysis

The uncertainties in the measured quantities propagate through all calculations of the derived quantities. Hence, an uncertainty analysis was performed to estimate these uncertainties. This analysis is based on the method suggested by Kline and McClintock [23]. The results are $\dot{m}$, ±2.0%; G, ±2.3%; Re, ±2.4%; q'', ±5.1%; and x, ±5.8%.

8 Results and Discussion

Experiments were conducted to determine the CHF condition over a range of exit pressures, mass fluxes, and inlet subcoolings in a single stainless steel tube of inside diameter 0.427 mm. The experimental conditions are given in Table 1.

Single-phase experiments were first performed to check for the energy balances. The guard heater power was controlled during both the single- and two-phase experiments. The single-phase pressure drop was found to be in very good agreement with well established theory. The ratio of the total pressure drop (sum of the pressure drops at the entrance, in the developing flow region, fully developed region, and the exit) from the experiment to that calculated using correlations from the literature was within ±6%, as can be seen in Fig. 3.

During the single-phase heat transfer experiments, the flow was hydrodynamically fully developed but was thermally developing through the length of the heated section. The heat transfer results were compared with the modified Hausen correlation (for constant heat flux) given below.

$$\text{Nu} = 4.36 + \frac{0.19(\text{Re Pr } D/L)^{0.8}}{1 + 0.117(\text{Re Pr } D/L)^{0.467}} \tag{9}$$

This correlation overpredicted the data by about 34% at lower Reynolds number (Re ~ 200) but underpredicted it by about 50% at Re ~ 1200. These laminar single-phase heat transfer results are consistent with other results from the literature [24,25]. In the two-phase study, there were 50 CHF data points obtained. These include some data points where the characteristic wall temperature rise associated with the CHF condition was not observed. This will be discussed later in this section.

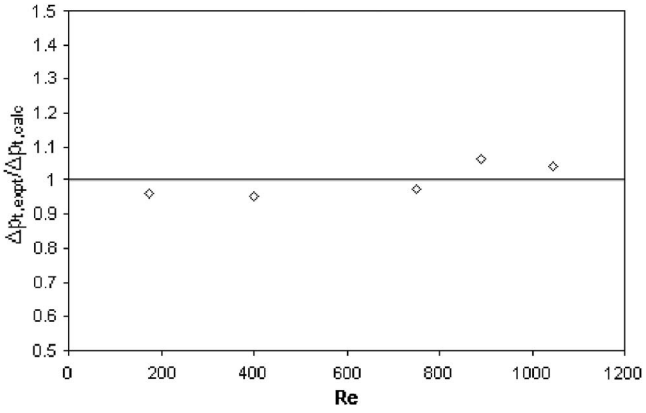

Fig. 3 $\Delta p_{t,expt}/\Delta p_{t,calc}$ **versus Re during single-phase flow experiment**

8.1 Flow Condition During the Critical Heat Flux Experiments. Flow was stabilized during the CHF experiments by maintaining a very high pressure drop (130–200 kPa) upstream of the test section through use of an inlet throttle valve; the rotameter float position was constant. A thermocouple mounted on the test-section wall just before the heated section did not show any variations in temperature (the temperature was very close to the inlet water temperature), which indicated that there was no backflow of vapor or axial conduction outward from the heated section. The pressure drop showed only small fluctuations with time (single- and two-phase flow regimes) except for very close to the CHF condition. One such plot of pressure drop versus time, at subatmospheric pressure and a mass flow rate of 560 kg/m^2 s, is shown in Fig. 4. The magnitude of the fluctuations in Fig. 4 was typical of all tests.

8.2 Wall Temperature Variations With Heat Flux. For the flow boiling tests, there was a characteristic sharp rise in wall temperature at the point of CHF, as can be seen in the plot of wall superheat versus heat flux depicted in Fig. 5. Note, also, that prior to the initiation of the CHF condition, often the wall temperature initially jumped up by about 35 °C, then dropped back; with further increases in heat flux, the CHF condition was reached (wall temperature was approximately 165 °C). At this point, test-section power was automatically shut off to prevent test-section damage.

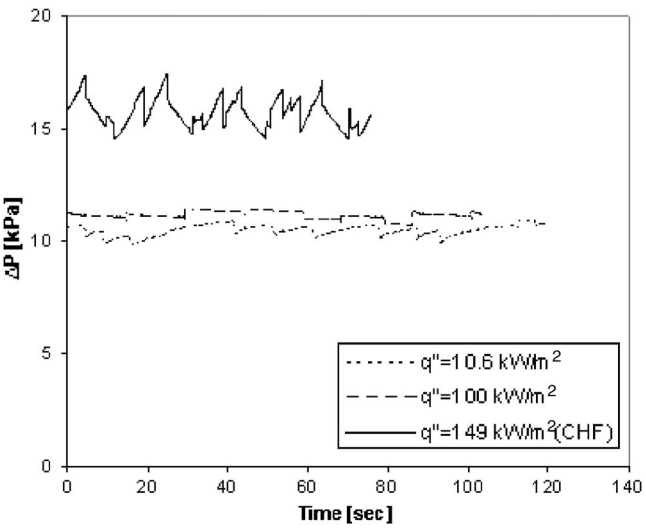

Fig. 4 Pressure drop versus time for G**=560 kg/m² s,** ΔT_{sub} **=38 °C,** P_{exit}**=25 kPa**

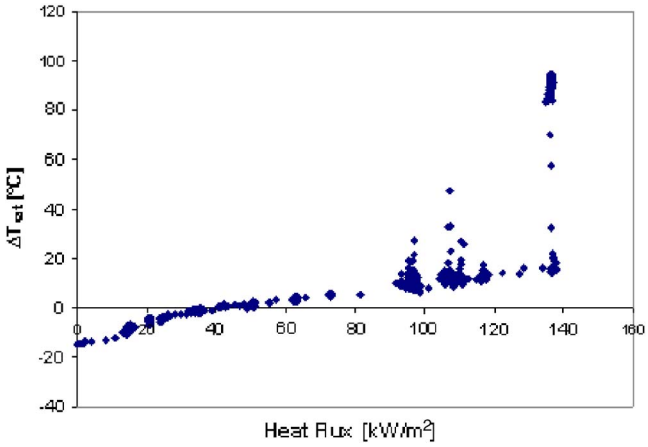

Fig. 5 Wall superheat versus heat flux (P_{exit}**=25 kPa;** G **=315 kg/m² s;** ΔT_{sub}**=15 °C)**

A similar observation was made in other tests with lower mass fluxes where the steady increase in heat flux caused the wall temperatures to increase by about 40–50 °C and then fall back before finally attaining the CHF condition. The jumps in the wall temperature just prior to CHF could be due to the occurrence of dry patches on the tube wall and when the liquid occasionally rewetted the wall, the temperatures would fall back. CHF would occur near the exit when the tube wall became completely dry. Lazarek and Black [13] observed a similar wall temperature response during CHF tests in a 3.1 mm diameter tube at a mass flux of about 270 kg/m^2 s. In experiments with higher mass fluxes, the wall temperatures did not exhibit such a sharp intermediate jump, but steadily increased until the CHF condition, with its characteristic temperature rise was reached, similar to that observed with lower mass fluxes.

Figure 6 shows the wall temperatures at six locations along the length of the heated section for two different conditions. For the lower pressure data, it is clear that the CHF occurred toward the exit of the heated section at which point the wall temperatures are considerably higher compared to those closer to the inlet of the test section.

The characteristic CHF did not occur for some of the experiments up to high heat fluxes, at which point power was shut down

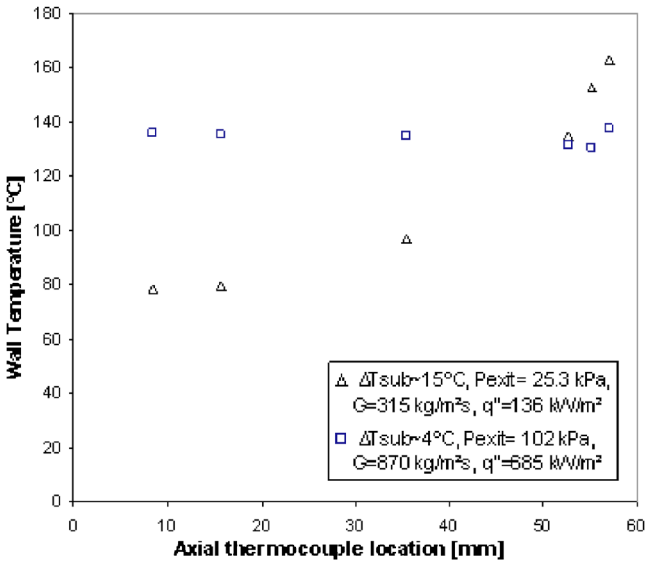

Fig. 6 Axial wall temperature variation (P_{exit}**=25 kPa, 102 kPa)**

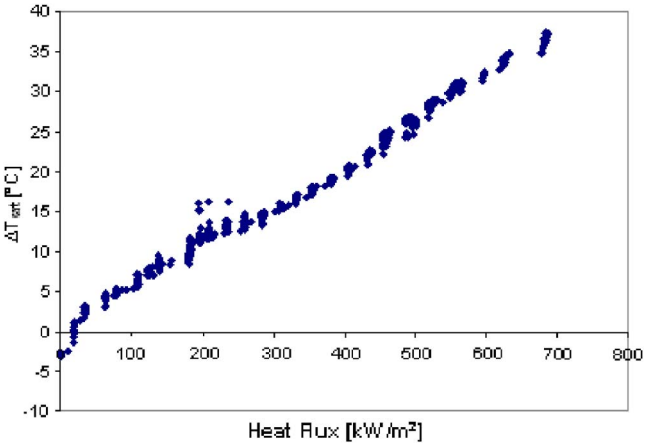

Fig. 7 Wall superheat versus heat flux (P_{exit}=102 kPa; G =870 kg/m^2 s; $\Delta T_{sub}\sim 4°C$)

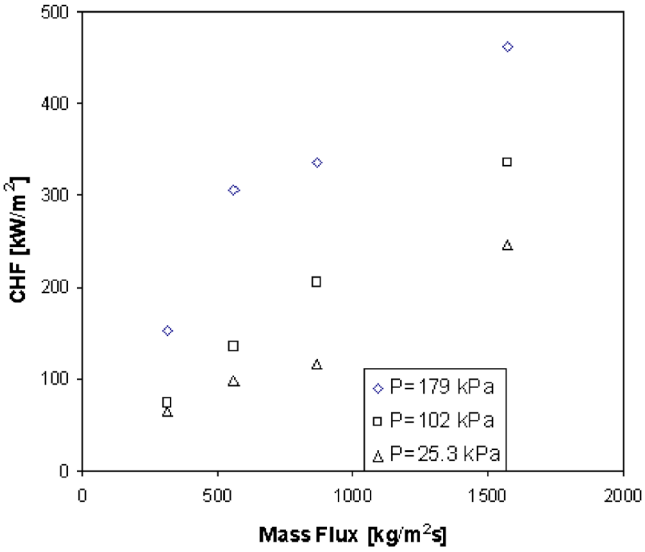

Fig. 8 Effect of mass flux on CHF for $\Delta T_{sub}\sim 46°C$, L_h =59 mm

so that the test sections were not destroyed. This happened for some of the tests carried out at low values of inlet subcooling (ΔT_{sub}=2–7°C). Figure 7 shows the exit wall temperature variation with heat flux at an exit pressure of 102 kPa, and one axial temperature data set is also shown in Fig. 6. The wall temperature linearly increased with heat flux but there was no sudden wall temperature spike as is normally associated with the CHF condition. Other tests conducted for slightly lower mass fluxes (e.g., G=560 kg/m^2 s) showed the wall temperature to suddenly increase (by about 30°C) and fall back a few times during the experiment but no characteristic CHF was observed. It might be possible that the flow transitions to an "inverted annular" type even at lower heat flux levels and the boiling takes place through the stable vapor film. The distinct boiling plateau was not seen during such tests. During this "film" type of boiling, the wall temperatures linearly increased as the heat flux was raised. More tests need to be conducted and further studies need to be done to confirm this phenomenon. Experiments performed at higher (179 kPa) and lower (25.3 kPa) exit pressures showed a similar trend but the wall temperature plots for these have been excluded for brevity. Roach et al. [10] made a similar observation of wall temperature behavior in some of their tests with single uniformly heated minitubes and attributed the disappearance of CHF to smooth transition of heat transfer from nucleate to film boiling. They found this to occur at mass fluxes as low as about 500 kg/m^2 s. Fukuyama and Hirata [26] reported similar findings in their studies with R-113 in a 1.2 mm inside diameter tube, but at relatively high mass fluxes (>40,000 kg/m^2 s) and high pressures (350–1500 kPa), and concluded that the traditional discontinuity in heat transfer coefficient between the nucleate and film boiling at the transition can be completely eliminated by the combined effects of mass flux, subcooling, and pressure. Similarly, Hosaka et al. [27] observed that compared to low mass flux flows, there was a smoother transition from nucleate to film boiling under the conditions of very high mass flux and high subcoolings in their tests with R-113 in tubes of 0.5 mm and 1 mm inside diameters.

For studies with the lower values of mass fluxes, a very high value of CHF was observed when inlet subcooling was very low resulting in exit qualities of about 0.2. But, for similar exit qualities in studies with higher mass fluxes, no CHF was observed. This is discussed in a later section describing the parametric effects on the CHF condition.

In all such tests at qualities slightly above zero when the characteristic CHF condition did not occur, the wall temperatures were much higher above the saturation temperature, and there was little variation in wall temperature from the inlet to the exit of the heated section as is depicted in Fig. 6 for the study at atmospheric pressure. Also, the wall temperature increased linearly as the heat flux was increased. For this reason, very few saturated CHF data points could be obtained and, in some tests, the experiment had to be terminated if wall superheats were above 60°C to save the test section even if no CHF was observed.

8.3 Parametric Effects on the Critical Heat Flux Condition

8.3.1 Effect of Mass Flux on Critical Heat Flux. Figure 8 depicts the dependence of CHF on mass flux for the three different exit pressures with inlet subcooling, $\Delta T_{sub}\sim 46°C$. The subcooled CHF condition was observed in these data at the three pressures. The CHF increases with an increase in mass flux. The CHF increases with an increase in exit pressure for the same value of mass flux; the slope of the CHF-G curves increases with pressure. A similar observation was made at other values of inlet subcooling.

8.3.2 Effect of Inlet Subcooling on Critical Heat Flux. The effect of inlet subcooling on CHF is shown in Fig. 9 for all exit pressures for two mass fluxes. For the higher mass flux, it is seen that, at higher levels of inlet subcooling, CHF slightly decreased with a decrease in inlet subcooling. But, at lower subcoolings (water inlet temperature close to the saturation temperature), the CHF increased with a decrease in subcooling. The same trend was observed at the three different pressures; the value of CHF was higher for the higher exit pressure. A similar behavior is observed for the lower mass flux as well. For the cases where the CHF dramatically increased with reduction in inlet subcooling, the exit quality at CHF was close to zero.

8.3.3 Effect of Exit Quality on Critical Heat Flux. Detailed results for the effect of exit quality on CHF are presented in Figs. 10–12. Note that, in Fig. 10, the CHF first decreases with an increase in quality in the subcooled region, but with a further increase in quality (near zero quality and above), the CHF is found to have an increasing trend with quality. Much higher values of CHF are found in the region close to saturation when compared to the high subcooled region. With still further increases in heat flux/exit quality, the CHF condition did not occur even when the wall superheat ($\Delta T_{sat}=T_w$-T_{sat}) reached about 40–60°C; the wall temperature increased essentially linearly with increases in heat flux. At this point, the experiment was terminated to save the

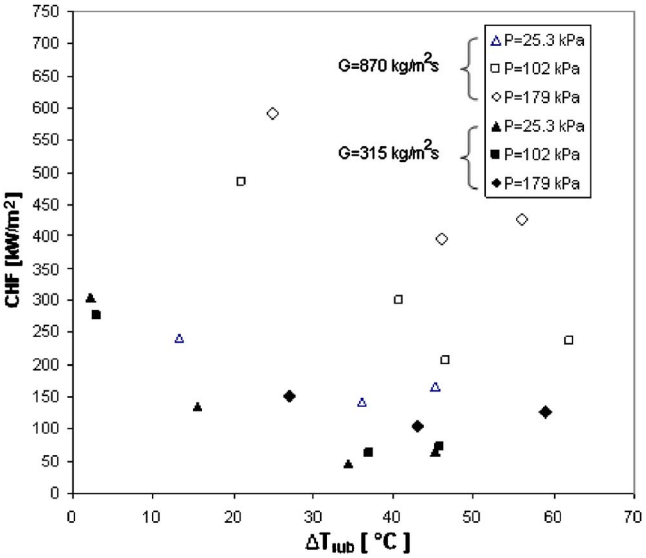

Fig. 9 Effect of inlet subcooling on CHF

test section, and the exit qualities and heat fluxes were $x=0.12$, $q''=825.2$ kW/m^2, and $\Delta T_{sat}=52°C$ for $G=1570$ kg/m^2 s; $x=0.19$, $q''=684.7$ kW/m^2, and $\Delta T_{sat}=37°C$ for $G=870$ kg/m^2 s;

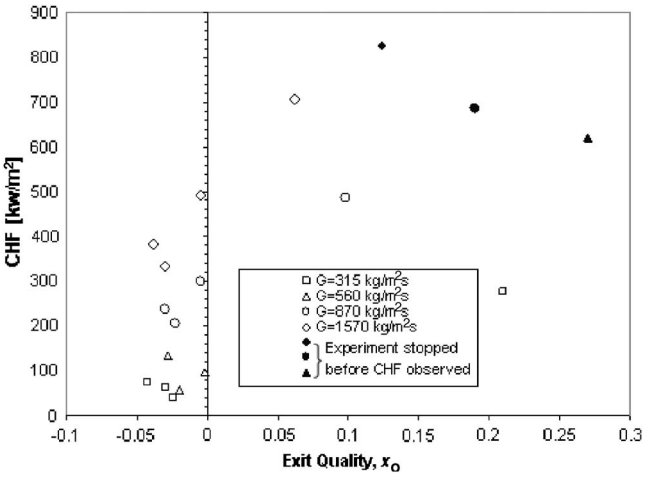

Fig. 10 Variation of CHF with quality for $P_{exit}=102$ kPa (abs)

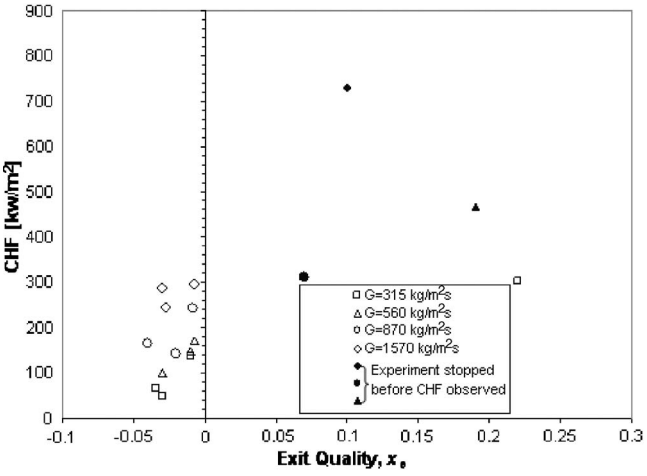

Fig. 11 Variation of CHF with quality for $P_{exit}=25$ kPa (abs)

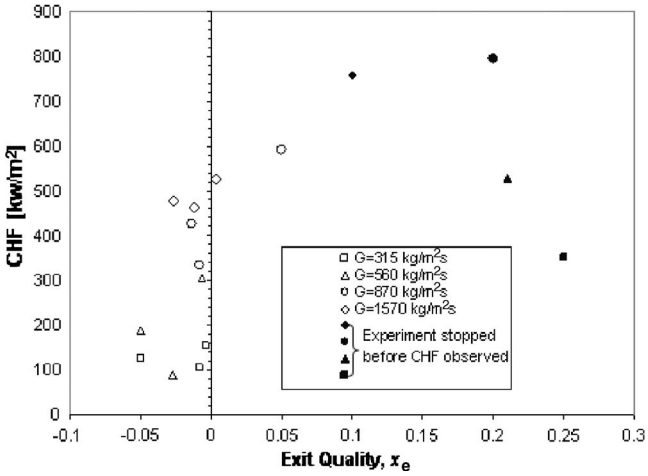

Fig. 12 Variation of CHF with quality for $P_{exit}=179$ kPa (abs)

and $x=0.27$, $q''=619$ kW/m^2, and $\Delta T_{sat}=55°C$ for $G=560$ kg/m^2 s. CHF was, however, observed at about $x=0.21$ for the mass flux of $G=315$ kg/m^2 s. The results for the exit quality are consistent with the trends observed for the variation of CHF with inlet subcooling.

The increase in CHF from the subcooled to the saturated region can be attributed to the void fraction change. In such a small diameter of the tube, the void fraction becomes significant enough to cause an increase in the velocity of flow through the tube, thereby causing an increase in the value of CHF. Nariai et al. [8] reported a similar observation in their studies on CHF in mini-tubes (1–3 mm inside diameter) but with much higher mass fluxes (7000–11,000 kg/m^2 s). The maximum exit quality in their data was 0.05. Bergles and Rohsenow [9] reported similar findings for flow of water through a 2.38 mm tube with a mass flux of 3000 kg/m^2 s.

Studies at subatmospheric pressure show a similar trend (Fig. 11). The CHF decreases with quality in the subcooled region, but as the quality advances toward zero, the CHF starts increasing again. No CHF was observed and the experiment was stopped when $x=0.1$ and $q''=727.6$ kW/m^2 for $G=1570$ kg/m^2 s, $x=0.07$ and $q''=312.6$ kW/m^2 for $G=870$ kg/m^2 s, and $x=0.19$ and $q''=465.5$ kW/m^2 for $G=560$ kg/m^2 s (for these cases, the inlet subcooling was about 3°C). For $\Delta T_{sub}=2.3°C$ and $G=315$ kg/m^2 s, a value of $q''_{CHF}=303.5$ kW/m^2, similar to that at an exit pressure of 102 kPa, was obtained.

Results for the variation of CHF with exit quality for the exit pressure of 179 kPa are reported in Fig. 12. Here, too, a similar trend to that observed in Figs. 10 and 11, is seen. For inlet subcoolings around 7–8°C, CHF was not observed for either of the mass fluxes. The wall superheats were quite high (55–60°C) with exit qualities of $x=0.1$, 0.2, 0.21, and 0.25 for mass fluxes of 1570 kg/m^2 s, 870 kg/m^2 s, 560 kg/m^2 s and 315 kg/m^2 s, respectively.

9 Comparison of Critical Heat Flux Data With Existing Correlations

All the CHF data obtained in this study, subcooled as well as saturated, were compared with the existing correlations. The CHF data in the subcooled region were compared with the Hall and Mudawar correlation [28]. This is represented in Fig. 13. Some of the deviation is because the Hall and Mudawar correlation overpredicts the data at very high inlet subcoolings and also it does not take into account the increased CHF behavior seen in this study as the qualities approach zero.

As previously seen, very few CHF data points could be obtained in the saturated region, because the wall temperatures kept

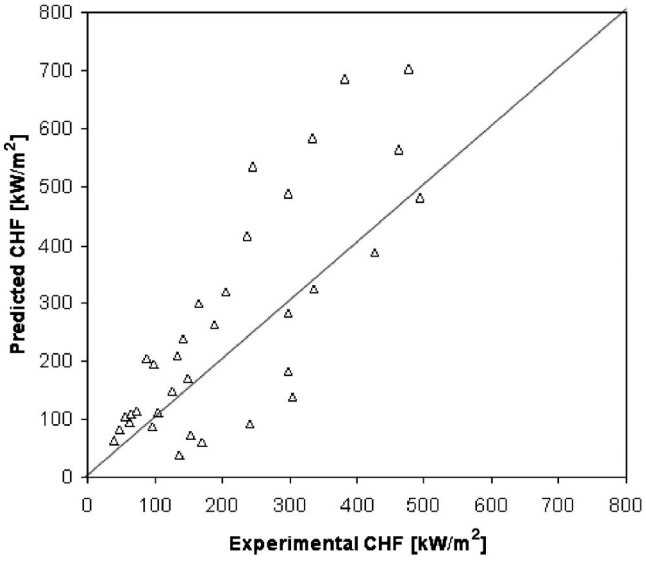

Fig. 13 Comparison of subcooled CHF data with the Hall and Mudawar correlation [28]

on linearly increasing with heat flux, and very high wall superheats were obtained even at significantly lower exit qualities. For most of the tests in the saturated region, the characteristic CHF was not observed and the experiment had to be terminated to save the test section. For the saturated CHF data, three correlations developed for mini/microchannels were considered for comparison: Wojtan et al. [19], Qu and Mudawar [29], and Zhang et al. [22]. The correlations from Refs. [19,29] do not consider the effect of inlet subcooling. However, the data presented in this study clearly show an effect of inlet subcooling on CHF. Hence, only one of these two correlations, by Qu and Mudawar [29], was used for comparison along with the correlation of Zhang et al. [22], which considers an inlet quality effect. The comparisons of the saturated CHF data with the correlations of Qu and Mudawar [29] and Zhang et al. [22] are shown in Fig. 14. The correlation of Zhang et al. highly overpredicts the data. It might be because this correlation was developed by doing a parametric trend analysis to the existing database of diameters in the range 0.33–6.22 mm. There are very few data that are available for the very small diameters, and they are almost all in the high mass flux range. The

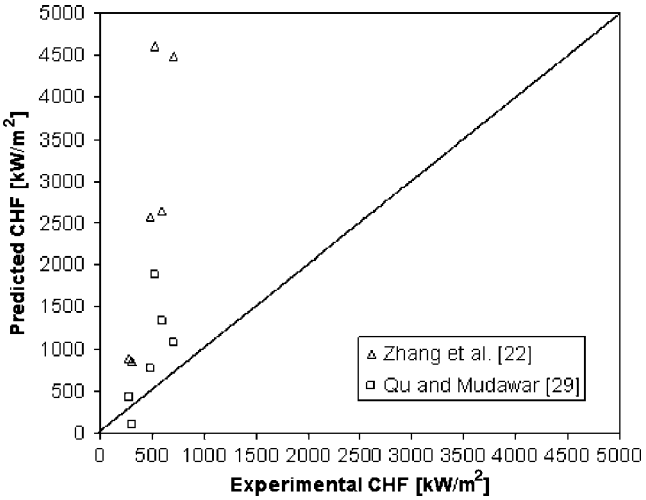

Fig. 14 Comparison of saturated CHF data with the Zhang et al. [22] and Qu and Mudawar correlations [29]

Qu and Mudawar correlation also does not predict the data well as it does not take into account the inlet subcooling effect.

Thus, there is a need for more data with smaller diameters for different mass fluxes, pressures, heated lengths, and type of fluids to develop a satisfactory CHF correlation, which can confidently predict CHF in the subcooled as well as the saturated region.

10 Conclusions

Experiments were performed to measure the CHF condition in the subcooled as well as the saturated region for a single microtube. The CHF increases with an increase in mass flux for all the three exit pressures considered in this study. For the same mass flux, CHF increased with an increase in exit pressure. Subcooling has a large impact on CHF at very low values of inlet subcooling. The effect of exit quality on CHF is found to be complicated. The CHF decreased with an increase in quality in the subcooled region, but suddenly increased to a high value around zero quality. With further increase in quality, CHF increased. The effects of other parameters on CHF, such as the fluid type, the diameter, and L/D ratio, need to be investigated. More experiments are being undertaken to fully understand the CHF phenomena in microtubes.

Acknowledgment

This work was supported by the National Science Foundation (NSF) under Grant No. CTS-0245642. Graduate student support from the Department of Mechanical, Aerospace and Nuclear Engineering at Rensselaer Polytechnic Institute is also gratefully acknowledged.

Nomenclature

D = tube inside diameter, mm
G = mass flux, $kg/m^2\,s$
H = heat gain, W
I = current, A
L = tube length, mm
Nu = Nusselt number
P = pressure, Pa
Pr = Prandtl number
PW = power, W
Q = volumetric flow rate, m^3/s
Re = Reynolds number
T = temperature, °C
V = voltage, V
c_p = specific heat of the fluid, J/kg K
h = specific enthalpy, J/kg
k = thermal conductivity, W/mK
$\dot{m}$ = mass flow rate, kg/s
q'' = heat flux, kW/m^2
x = quality

Greek Letters

Δp = pressure difference, Pa
ΔT = temperature difference, °C
ρ = density of fluid, kg/m^3

Subscripts

CHF = critical heat flux
TS = test section
calc = calculated
exit = at the exit
expt = from experiment
f = fluid
fg = liquid vapor
h = heated
i = inlet
o = outlet
in = inner

out = outer
sat = saturation
sh = shunt
sub = subcooled inlet
t = total
w = wall

References

[1] Moore, G., 1965, "Cramming More Components Onto Integrated Circuits," Electronics, **38**(8), pp. 114–117.

[2] Hannemann, R. J., 2003, "Thermal Control of Electronics: Perspectives and Prospects," *Rohsenow Symposium on Future Trends in Heat Transfer*, Warren M. Rohsenow Heat and Mass Transfer Laboratory, Massachusetts Institute of Technology, Cambridge, MA.

[3] Kakac, S., and Liu, H., 1998, *Heat Exchangers: Selection, Rating and Thermal Design*, CRC, Boca Raton, FL, Chap. 9, pp. 903–904.

[4] Kandlikar, S. G., and Grande, W. J., 2003, "Evolution of Microchannel Flow Passages—Thermohydraulic Performance and Fabrication Technology," Heat Transfer Eng., **24**(1), pp. 3–17.

[5] Vandervort, C. L., Bergles, A. E., and Jensen, M. K., 1994, "An Experimental Study of Critical Heat Flux in Very High Heat Flux Subcooled Boiling," Int. J. Heat Mass Transfer, **37**, pp. 161–173.

[6] Celata, G. P., Cumo, M., and Mariani, A., 1993, "Burnout in Highly Subcooled Water Flow Boiling in Small Diameter Tubes," Int. J. Heat Mass Transfer, **36**(5), pp. 1269–1285.

[7] Celata, G. P., Cumo, M., and Mariani, A., 1997, "Geometrical Effects on the Subcooled Flow Boiling Critical Heat Flux," Rev. Gen. Therm., **36**, pp. 807–814.

[8] Nariai, H., Inasaka, F., and Uehara, K., 1989, "Critical Heat Flux in Narrow Tubes with Uniform Heating," Heat Transfer-Jpn. Res., **18**, pp. 21–30.

[9] Bergles, A. E., and Rohsenow, W. M., 1962, "Forced-Convection Surface-Boiling Heat Transfer and Burnout in Tubes of Small Diameter," Massachusetts Institute of Technology Report No. AF 19(604)-7344; U.S. Atomic Energy Commission DSR Report 8767-21.

[10] Roach, G. M., Jr., Abdel-Khalik, S. I., Ghiaasiaan, S. M., Dowling, M. F., and Jeter, S. M., 1997, "Low Flow Critical Heat Flux in Heated Microchannels," Nucl. Sci. Eng., **131**, pp. 411–425.

[11] Oh, C. H., and Englert, S. B., 1993, "Critical Heat Flux for Low Flow Boiling in Vertical Uniformly Heated Thin Rectangular Channels," Int. J. Heat Mass Transfer, **36**(2), pp. 325–335.

[12] Lowdermilk, W. H., Lanzo, C. D., and Siegel, B. L., 1958, "Investigation of Boiling Burnout and Flow Instability for Water Flowing in Tubes," Report No. NACA-TN-4382.

[13] Lazarek, G. M., and Black, S. H., 1982, "Evaporative Heat Transfer, Pressure Drop and Critical Heat Flux in a Small Vertical Tube with R-113," Int. J. Heat Mass Transfer, **25**(7), pp. 945–960.

[14] Bowers, M. B., and Mudawar, I., 1994, "High Flux Boiling in Low Flow Rate, Low Pressure Drop Mini-Channel and Micro-Channel Heat Sinks," Int. J. Heat Mass Transfer, **37**(2), pp. 321–332.

[15] Yu, W., France, D. M., Wambsganss, M. W., and Hull, J. R., 2002, "Two-Phase Pressure Drop, Boiling Heat Transfer, and Critical Heat Flux to Water in a Small-Diameter Horizontal Tube," Int. J. Multiphase Flow, **28**, pp. 927–941.

[16] Kamidis, D. E., and Ravigururajan, T. S., 1999, "Single and Two-Phase Refrigerant Flow in Mini-Channels," *Proceedings of NHTC2000: 33rd National Heat Transfer Conference*, Albuquerque, NM, pp. 1–8.

[17] Lezzi, A. M., Niro, A., and Beretta, G. P., 1994, "Experimental Data on CHF for Forced Convection Water Boiling in Long Horizontal Capillary Tubes," *Proceedings of the Tenth International Heat Transfer Conference*, Rugby, UK, Vol. 7, pp. 491–496.

[18] Jiang, L., Wong, M., and Zohar, Y., 1999, "Phase Change in Microchannel Heat Sinks with Integrated Temperature Sensors," J. Microelectromech. Syst., **8**, pp. 358–365.

[19] Wojtan, L., Revellin, R., and Thome, J. R., 2006, "Investigation of Saturated Critical Heat Flux in a Single Uniformly Heated Microchannel," Exp. Therm. Fluid Sci., **30**, pp. 765–774.

[20] Kuan, W. K., and Kandlikar, S. G., 2006, "Critical Heat Flux Measurement and Model for Refrigerant-123 Under Stabilized Flow Conditions in Microchannels," ASME Paper No. IMECE2006-13310.

[21] Koşar, A., Kuo, C.-J., and Peles, Y., 2005, "Reduced Pressure Boiling Heat Transfer in Rectangular Microchannels With Interconnected Reentrant Cavities," ASME J. Heat Transfer, **127**, pp. 1106–1114.

[22] Zhang, W., Hibiki, T., Mishima, K., and Mi, Y., 2006, "Correlation of Critical Heat Flux for Flow Boiling of Water in Mini-Channels," Int. J. Heat Mass Transfer, **49**, pp. 1058–1072.

[23] Kline, S. J., and McClintock, F. A., 1953, "Describing Uncertainties in Single Sample Experiments," Mech. Eng. (Am. Soc. Mech. Eng.), **75**, pp. 3–8.

[24] Celata, G. P., Cumo, M., Guglielmi, M., and Zummo, G., 2002, "Experimental Investigation of Hydraulic and Single-Phase Heat Transfer in 0.13-mm Capillary Tube," Microscale Thermophys. Eng., **6**, pp. 85–97.

[25] Peng, X. F., and Peterson, G. P., 1996, "Convective Heat Transfer and Flow Friction for Water Flow in Microchannel Structures," Int. J. Heat Mass Transfer, **39**, pp. 2599–2608.

[26] Fukuyama, Y., and Hirata, H., 1982, "Boiling Heat Transfer Characteristics With High Mass Flux and Disappearance of CHF Following to DNB," *Proceedings of the Seventh International Heat Transfer Conference*, Hemisphere, Washington, DC, Vol. 4, pp. 273–278.

[27] Hosaka, H., Mirata, M., and Kasagi, N., 1990, "Forced Convective Subcooled Boiling Heat Transfer and CHF in Small Diameter Tubes," *Proceedings of the Ninth International Heat Transfer Conference*, Hemisphere, Washington, DC, Vol. 2, pp. 129–134.

[28] Hall, D. D., and Mudawar, I., 2000, "Critical Heat Flux (CHF) for Water Flow in Tubes-II. Subcooled CHF Correlations," Int. J. Heat Mass Transfer, **43**, pp. 2605–2640.

[29] Qu, W., and Mudawar, I., 2004, "Measurement and Correlation of Critical Heat Flux in Two-Phase Micro-Channel Heat Sinks," Int. J. Heat Mass Transfer, **47**, pp. 2045–2059.